Remote Sensing of Environment 182 (2016) 60–71

Contents lists available at ScienceDirect

Remote Sensing of Environment

journal homepage: www.elsevier.com/locate/rse

Incorporating plant phenological trajectory in exotic saltcedar detection with monthly time series of Landsat imagery

Chunyuan Diao, Le Wang *

Department of Geography, University at Buffalo, the State University of New York, 105 Wilkeson Quad, Buffalo, NY 14261, USA

ARTICLE INFO

Article history:
Received 10 September 2015
Received in revised form 15 April 2016
Accepted 30 April 2016
Available online 19 May 2016

Keywords:
Saltcedar
Landsat
Intra-annual phenology
Image classification
Feature selection
Random Forest

ABSTRACT

Over the past century, non-native saltcedar (*Tamarix* spp.) has expanded into most of riparian zones of the southwestern United States and posed significant threats to the native biotic communities. Repeated monitoring of saltcedar distribution over region-wide geographic areas is urgently essential for conservation agencies to develop cost-effective control strategies. Current studies have mostly concentrated on the mapping of saltcedar distribution with a single remote sensing image acquired during its leaf senescence. Given the phenological variation within saltcedar and the spectral confusion between saltcedar and natives, our ability to detect saltcedar with a single-date image is still limited. The objective of this study was to develop new intra-annual phenology-based strategies to detect exotic saltcedar with monthly time series of Landsat imagery. Several temporal phenology-based detection strategies (i.e., phenological bands, phenological NDVI, and phenological metrics) that could track the intra-annual phenological trajectory of plants were devised. With the proposed detection strategies, crucial months and phenological stages in saltcedar detection were investigated. Results indicated that the proposed strategy of phenological bands could accommodate the phenological variation within saltcedar and improve the classification accuracy significantly. Several phenological stages (e.g., flowering and leaf senescence) were deemed as important in discriminating saltcedar from other riparian plants at the Landsat scale. The proposed strategy was found to be relatively robust to the lack of a single Landsat image. It is concluded that monthly time series of Landsat imagery are promising in facilitating the long-term mapping of saltcedar distribution over extended areas.

1. Introduction

Invasive species threaten the functioning of natural ecosystems and cause substantial economic losses at the global scale. Among a number of exotic plants, saltcedar (*Tamarix* spp.), a woody shrub, is particularly problematic in the southwestern United States and has levied significant impacts on the riparian ecosystems over the past century (Zavaleta, 2000). Deliberately introduced to United States, saltcedar is now envisaged as the third most frequently occurring woody riparian plant in the western US (Friedman et al., 2005). The widespread invasions of saltcedar have been indicted for altering fire regimes, increasing soil salinity, depleting river flows, and reducing recruitment of native plants (Di Tomaso, 1998; Hart, White, McDonald, & Sheng, 2005). Millions of dollars are spent annually by local, state, and federal agencies eradicating and controlling this exotic plant (Follstad Shah, Dahm, Gloss, & Bernhardt, 2007). One control technique that has garnered considerable attention is the use of biological control agent (saltcedar leaf beetle, *Diorhabda* spp.) to defoliate saltcedar (Hultine et al., 2009). However, recently the negative perceptions of saltcedar have been challenged by new research findings, and the role of saltcedar in ecosystem function and habitat degradation has been called for reevaluation (Glenn & Nagler, 2005; Shafroth et al., 2005; Stromberg, Chew, Nagler, & Glenn, 2009). Accurately mapping the spatial distribution of saltcedar is indispensably crucial for conservation agencies to reframe the view of this introduced plant and to undertake systemic restoration of riparian ecosystems (Nagler, Glenn, Jarnevich, & Shafroth, 2011; Stromberg et al., 2009).

Remote sensing offers valuable opportunities to detect saltcedar and monitor its geographical distributions. Drawing on the information from spectral, temporal or spatial domains, researchers have explored remote sensing with extensive efforts to map plant distributions in various ecosystems (Bradley, 2014; Diao & Wang, 2014; He, Rocchini, Neteler, & Nagendra, 2011; Wang & Zhang, 2014). Yet remote detection of invasive plants to date has not been a painless task since many different plants share similar spectral signatures, phenological patterns or spatial textures. Capturing unique features of saltcedar that permit it to be distinguished from surrounding native vegetation is key to developing operational monitoring protocols for this exotic plant along riparian corridors. A particularly desirable feature for characterizing saltcedar is its distinct spectral signature (or foliage color) during the leaf senescence stage (Everitt & Deloach, 1990; Wang, Silván-Cárdenas,

* Corresponding author.
E-mail addresses: chunyuan@buffalo.edu (C. Diao), lewang@buffalo.edu (L. Wang).

http://dx.doi.org/10.1016/j.rse.2016.04.029
0034-4257/

Yang, & Frazier, 2013). Saltcedar leaves at this time window turn a yellow-orange color and can be more easily distinguished from the greenish or darker tones of associated native vegetation (e.g., willow and mesquite). Consequently, this optimal time window has been favored by researchers to investigate the role of remote sensing images in mapping the spatial distribution of saltcedar in various riparian zones (Diao & Wang, 2014; Evangelista, Stohlgren, Morisette, & Kumar, 2009; Hamada, Stow, Coulter, Jafolla, & Hendricks, 2007; Narumalani, Mishra, Burkholder, Merani, & Willson, 2006; Rundquist & Brookman, 2007; Silván-Cárdenas & Wang, 2010; Wang et al., 2013; Yang, Everitt, & Fletcher, 2013; Ji & Wang 2016).

In recent years, the increasing proliferation of high-spatial resolution airborne platforms has aided in the remote detection of invasive plants. Aerial photos and high resolution hyperspectral imagery (e.g., Airborne Imaging Spectroradiometer for Applications (AISA)), acquired within the optimal time window, have been employed to distinguish senescent saltcedar from native species with satisfactory classification accuracy (Everitt & Deloach, 1990; Hamada et al., 2007; Wang et al., 2013). Despite the detailed plant information discernable with airborne sensors, the high cost and limited coverage of these images have hampered their application in saltcedar mapping over large geographical areas (Lass et al., 2009). To facilitate the region-wide monitoring of saltcedar invasion, the spaceborne Landsat image acquired during the early winter has recently been investigated for mapping senescent saltcedar in Texas (Silván-Cárdenas & Wang, 2010; Wang et al., 2013). This single-image-based detection result indicated that Landsat imagery is promising in mapping large, dense patches of saltcedar across the landscape at the regional scale. However, there are three issues with the single-image-based detection strategy. First, plants in various phenological stages may exist in a single Landsat image. The single image acquired within the optimal time window is primarily used for detecting senescent saltcedar via its distinct spectral characteristic. The potential spectral confusion between saltcedar in other stages (e.g., leaf-on or leaf-off stage) and native species, may dramatically compromise detection accuracy, especially in heterogeneous landscapes. Second, despite the importance of leaf senescence in saltcedar detection, other phenological characteristics (e.g., flowering) may contribute to the discrimination among the plants. A single remotely sensed image cannot take into account all essential phenological characteristics. Third, the availability of the single Landsat image within the optimal time window is not assured. The optimal time window lasts only three or four weeks (Yang et al., 2013). Given the 16-day revisit cycle of Landsat, the detection success is notably limited by the quality of few images.

The aforementioned issues point to the need for exploring a more comprehensive suite of features that could improve detection of exotic saltcedar from remotely sensed imagery. Plant phenology is a temporal feature that portrays the seasonal growth and development of vegetation, and offers insights into plant physiological activities at various stages (e.g., leaf elongation, bud differentiation, flowering, and leaf senescence) (Lieth, 1974). Phenological trajectory of plants can be established with the time series of satellite imagery through tracing the temporal variation in spectral reflectance over the course of the growing season (Morisette et al., 2008; Zhang et al., 2003). The extended observation period granted by the satellite imagery time series thus offers more opportunities to capture distinct temporal features that could improve classification accuracy. To date, remotely sensed time series analyses of vegetation dynamics have been mostly conducted with MODerate-resolution Imaging Spectroradiometer (MODIS), Advanced Very High Resolution Radiometer (AVHRR), and SPOT Vegetation (VGT) imagery (Kerr & Ostrovsky, 2003; Morisette

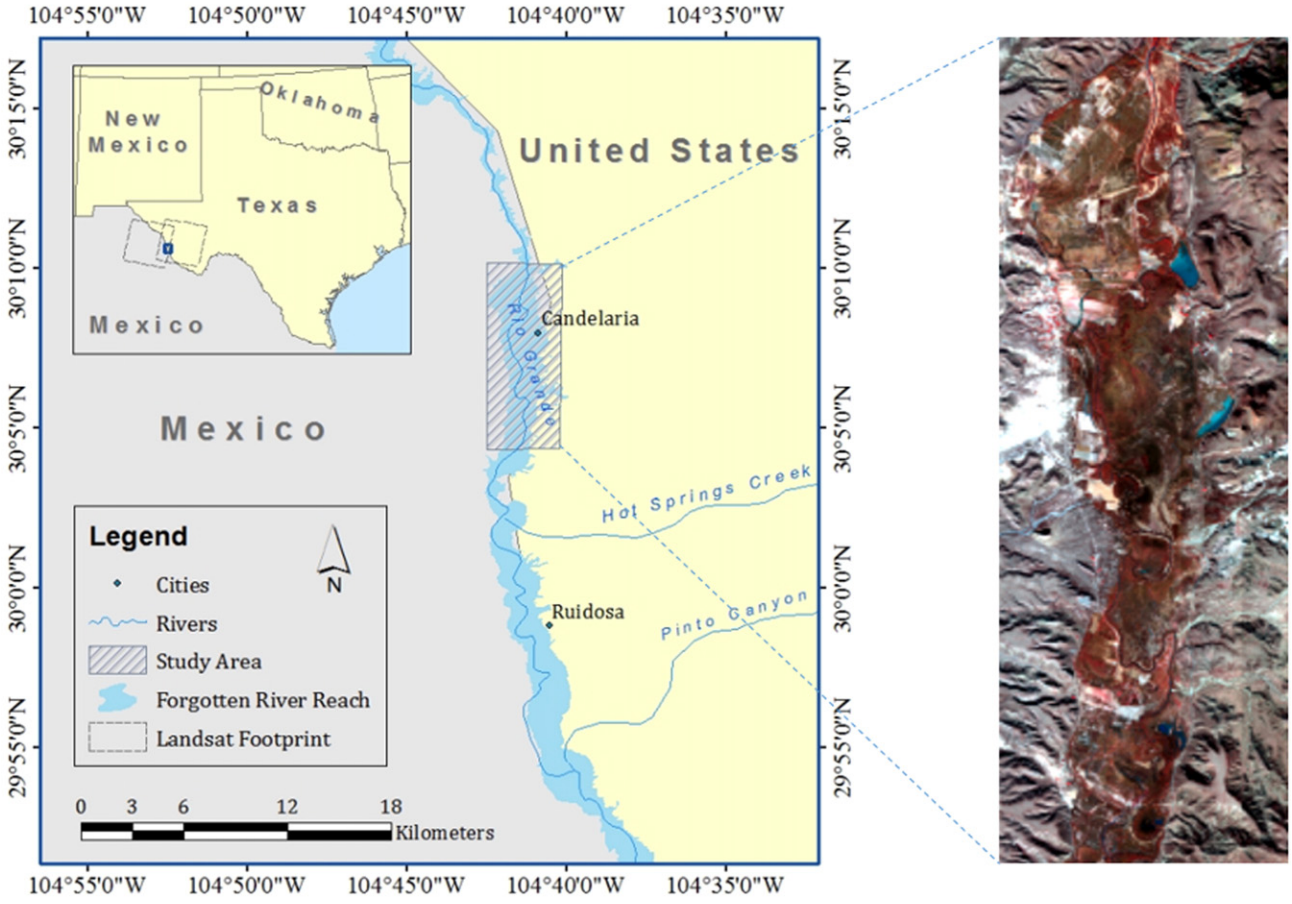

Fig. 1. Geographic location of the study area. Two Landsat footprints (path/row 31/39 and 32/39) cover the study area. The false-color composite of Landsat imagery of the study area is shown on the right.

et al., 2008). Morisette et al. (2006) extracted three phenological features (i.e., mean, amplitude, and phase) from the MODIS time series to describe the seasonal variation of vegetation greenness, and used them to predict suitable habitats of saltcedar across their US range. Yet the phenology extracted by the time series of coarse spatial resolution MODIS imagery (250 m) is usually mixed by that of both native and non-native plants, especially in spatially diverse riparian zones.

Time series of Landsat imagery, with the spatial resolution of 30 m, are more suitable for capturing phenological dynamics of invasive plants in spatio-temporal complex landscapes (Bradley, 2014). Evangelista et al. (2009) used six Landsat images and derived vegetation indices at different times of the growing season to map exotic saltcedar along the Arkansas River in Colorado. The selected six Landsat images that accommodate the seasonal variation were found to be more effective in detecting saltcedar than a single image. However, the six Landsat images were acquired over five years (i.e., 1999–2003). The phenological variations of plants during this time period include both intra- and inter-annual variations. Given the fact that intra- and inter-annual plant phenology usually occurs at different temporal scales, it is desired to address intra- and inter-annual phenological variations separately (Hufkens et al., 2012). Besides, sometimes it is difficult to assume that the areas occupied by invasive plants remain unchanged within a number of years. Monitoring the saltcedar distribution on an annual basis is more promising to guide the effective management of plant invasions. Currently, most of intra-annual Landsat studies only use a very limited number of images (e.g., two Landsat images) to incorporate the seasonal variation in plant detection (Bradley, 2014; Peterson, 2005; Rapinel, Bouzillé, Oszwald, & Bonis, 2015; Singh & Glenn, 2009). It is still not clear how the rich information carried by the Landsat time series within a year can be efficiently utilized to characterize the phenological trajectory of invasive plants and facilitate the remote monitoring of saltcedar.

The objective of our research was to develop new intra-annual phenology-based strategies to detect and monitor the geographical distribution of exotic saltcedar with monthly Landsat imagery. Specifically, we sought to: 1) devise several intra-annual phenology-based detection strategies that could track the phenological trajectory of plants throughout the year (see Section 3.1), 2) investigate crucial months and seasons in characterizing the seasonal variation of saltcedar, and 3) evaluate the importance of the optimal time window in remotely detecting saltcedar.

2. Study site and data

2.1. Study site

The study site is located along the Forgotten River reach of the Rio Grande River near the town of Candelaria, Texas (Fig. 1). The study site covers an area of 5 km × 10 km centered at longitude 104.69°W and latitude 30.12°N. The Rio Grande River originates from the San Juan Mountains of southern Colorado, flows along the Mexico-United States border, and extends southward to the Gulf of Mexico. The segment of the Rio Grande stretching from Fort Quitman, Texas, to the confluence of the Rio Conchos near Presidio, Texas, is called the Forgotten River due to deteriorated riparian landscapes and excessive depletion of river flows. Impacted by anthropogenic water regulations and dam constructions, the hydrologic regimes and vegetation communities along the Forgotten River have been profoundly altered in the past century. The most notable change is the progressive replacement of native floodplain communities by saltcedar (Engel-Wilson & Ohmart, 1978). As a result, the vegetated riparian zone of the study site is primarily composed of saltcedar, with mixes of native mesquite (*Prosopis* spp.) and willow (*Salix* spp.). The colonization of saltcedar varies in density and extent across the study area, including both monotypic dense stands and sparse mixed patches. The native cottonwood (*Populus* spp.), that historically dominated the floodplain, has been completely eliminated.

2.2. Image acquisition and pre-processing

2.2.1. Landsat data

To devise new intra-annual phenology-based detection strategies, a monthly time series of Landsat images for the year 2005 were constructed. The monthly sampling rate was selected as the tradeoff between the temporal revisit frequency of Landsat and the intra-annual phenological dynamics of vegetation. The study site is covered by two adjacent overlapping Landsat footprints (path 31, row 39, and path 32, row 39) (Fig. 1). A total of 23 cloud-free Landsat Thematic Mapper (TM) images can be acquired for this site over the course of the year 2005 (Fig. 2). Given the acquisition time of these Landsat TM images, the image around the middle of each month was selected (or interpolated) to construct and approximate the equally spaced monthly time series. One exception is the month of December, which is deemed as the optimal time window to spectrally distinguish senescent saltcedar from natives. The image acquired in this month should be prioritized in devising the detection strategies. Yet no Landsat TM images are available in December, 2005. The Landsat Enhanced Thematic Mapper Plus (ETM+) images that contain data gaps due to the Scan Line Corrector (SLC) failure were also scrutinized. It is noted that the Landsat ETM+ SLC-off image acquired on December 26 is free of clouds and of good quality, and thus was selected in the subsequent time series analysis. However, the training and testing data for assessing the detection strategies were not sampled from the SLC-off gapped area to eliminate its influence on the evaluation results.

The monthly time series of Landsat images were co-registered to the reference data (i.e., AISA, see Section 2.2.2) with root mean square errors <0.2. Subsequently, the images were atmospherically corrected to surface reflectance with the Landsat Ecosystem Disturbance Adaptive Processing System (LEDAPS), using the 6S radiative transfer model (Masek et al., 2006). For each Landsat image, six spectral bands (i.e., band 1, 2, 3, 4, 5, and 7) with the spatial resolution of 30 m were used in this study.

2.2.2. Reference data

Due to the difficulty of collecting sufficient ground truth samples at the Landsat scale, the reference data for evaluating the efficacy of the competing detection strategies was obtained through the classified

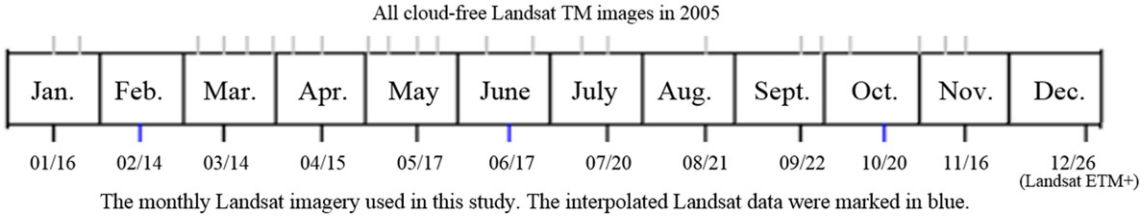

Fig. 2. Timeline of Landsat data available for the year 2005 in the study area.

AISA image. The AISA image was acquired on December 21, 2005, which coincided with the senescent stage of saltcedar and the leaf-off stage of native mesquite and willow (Everitt & Deloach, 1990; Yang et al., 2013). The image has a spatial resolution of 1 m, with 61 bands in the spectral range from 400 to 1000 nm. This detailed spectral and spatial information offered by the AISA image can help accommodate the within-class spectral variation and facilitate the differentiation between saltcedar and native species.

Two field trips were conducted in November 2004 and December 2005 to collect ground reference samples for classifying the AISA image. With a handheld GPS (Trimble GeoXM), the locations of typical land cover classes (i.e., saltcedar, native woody riparian species, non-woody vegetation, and other land cover types) were recorded (Table 1). An average of twenty points and ten polygons were obtained for each land cover type. Additional polygons for non-vegetated areas were manually delineated from the AISA image. Based on the extensive field reconnaissance, a two-level hierarchical classification scheme was designed. The scheme encompasses the most important land cover classes in our study area. Detailed land cover types within each general class (level I) were distinguished at level II. For example, saltcedar of various phenological stages (e.g., green, senescent, and leaf-off saltcedar) were examined at the level II classification exploratory stage. Investigation of phenological variation in the classification was imperative at such a fine spatial resolution to account for the within-class spectral variation and reduce the spectral confusion between classes.

Spectral Angel Mapper (SAM) was used to classify the AISA image at classification level II and assign each pixel to one of the land cover classes (Kruse et al., 1993). This classification method determines the spectral similarity between the image spectra and reference spectra (endmembers) in the spectral library via the spectral angle, and matches the image spectra to the class that forms the smallest angle. The reference spectral library was built from in-situ spectral signatures measured for target land cover types with a portable handheld spectroradiometer (ASD VNIR Field Spectrometer) during the field trips, supplemented by the endmembers extracted for non-vegetated classes directly from the AISA image. The SAM classification result was then aggregated to the classification level I. The overall accuracy, evaluated with ground reference samples (200 for each class), was 93.7%, and the kappa statistic was 0.91 (Table S1). Moreover, the classification result was spatially resampled to 30 m to match the resolution of Landsat imagery. The resampled pixels with the fraction of the main land cover type (i.e., saltcedar, native woody riparian species, or other) >50% were labeled as the reference data for evaluating the proposed Landsat-based strategies. In total there were 3350, 2734, and 7752 pixels for saltcedar, native species, and other, respectively. 50% of the samples for each class were randomly selected for training the models, and the remainder was reserved for testing.

Table 1
Two-level hierarchical classification scheme designed in this study.

Class level I	Class level II
Saltcedar	Green saltcedar (*Tamarix* spp.)
	Senescent saltcedar (*Tamarix* spp.)
	Leaf-off saltcedar (*Tamarix* spp.)
Native woody riparian species	Leaf-on willow (*Salix* spp.)
	Leaf-off willow (*Salix* spp.)
	Leaf-on mesquite (*Prosopis* spp.)
	Leaf-off mesquite (*Prosopis* spp.)
	Marshy weed (*Limnophila* spp.)
	Poverty weed (*Iva axillaris* Pursh)
Other	Green grasses
	Dry grasses
	Creosote bush (*Larrea tridentate*)
	Desert gravel
	Paved road
	Sand
	Roof
	Wetland
	Water (river, lake or pond)

3. Methods

This section introduces the main methods used to address our objectives (Fig. 3). First, four detection strategies were developed to characterize the intra-annual phenological trajectory of plants using the monthly Landsat time series. Second, two classification algorithms were employed to evaluate the four proposed detection strategies. Crucial months and seasons in characterizing the seasonal variability of saltcedar were explored. Additionally, the role of the optimal time window in the Landsat time series was evaluated. The performance of monthly Landsat imagery was compared to that of 11 months' imagery (except December) to determine if the image acquired in the optimal time window is indispensable to remotely detect saltcedar.

3.1. Four detection strategies

Based on the monthly Landsat time series, four detection strategies were developed: 1) using solely single-date Landsat imagery acquired within the optimal time window (i.e., the image acquired on December 26), 2) using the phenological bands (i.e., monthly Landsat bands), 3) using the phenological NDVI (i.e., monthly Landsat NDVI), and 4) using the phenological metrics (see Section 3.1.1) derived from the monthly Landsat images (Table 2). The single-date Landsat imagery provided a baseline for benchmarking the Landsat-based time series analysis. Three competing temporal profiles that characterize the intra-annual phenological dynamics of vegetation were investigated in this study.

3.1.1. Phenological metrics

As one proposed detection strategy, phenological metrics were extracted from the monthly Landsat NDVI time series over the course of the year 2005. The phenological metrics (e.g., timing of greenness onset and length of the vegetation season) are temporal markers to characterize the seasonal photosynthetic activity and phenological patterns of plants.

To extract phenological metrics, the monthly Landsat NDVI time series was first fitted with smoothing functions. The smoothing functions were used to suppress the short frequency variation and reduce the influence of outliers in the time series. Three smoothing functions were explored in this study, namely adaptive Savitzky-Golay function (Jönsson & Eklundh, 2004), asymmetric Gaussian function (Jönsson & Eklundh, 2002), and double logistic function (Beck, Atzberger, Høgda, Johansen, & Skidmore, 2006). The original time series curve was fitted with these three functions through least square optimization. We found that the adaptive Savitzky-Golay function exhibited better performance (i.e., smaller root mean square errors), compared to the other two functions. The adaptive Savitzky-Golay function fits the data to a local polynomial within a moving window, and allows data smoothing without forcing a given mathematical function (e.g., Gaussian or logistic curves). It was selected in this study to smooth the Landsat time series.

Eleven representative phenological features (Table 3), related to the growing seasons, were then extracted from the smooth time series using TIMESAT (Jönsson & Eklundh, 2004; Tan et al., 2011). The beginning of the growing season is a valley point for which the vegetation index begins to increase in a growing cycle. Similarly, the end of the growing season is the brown-down date, for which the vegetation index ends to decrease at the decaying end of a growing cycle. The base NDVI value is indicative of soil background conditions. The peak NDVI value is associated with the seasonal highest amount of vegetation greenness, and the amplitude denotes the variation and seasonal range of greenness during the growing period. The left derivative is the rate of green-up and plant growth, and is theoretically related to the physiognomy of vegetation. Similarly, the right derivative denotes the rate of

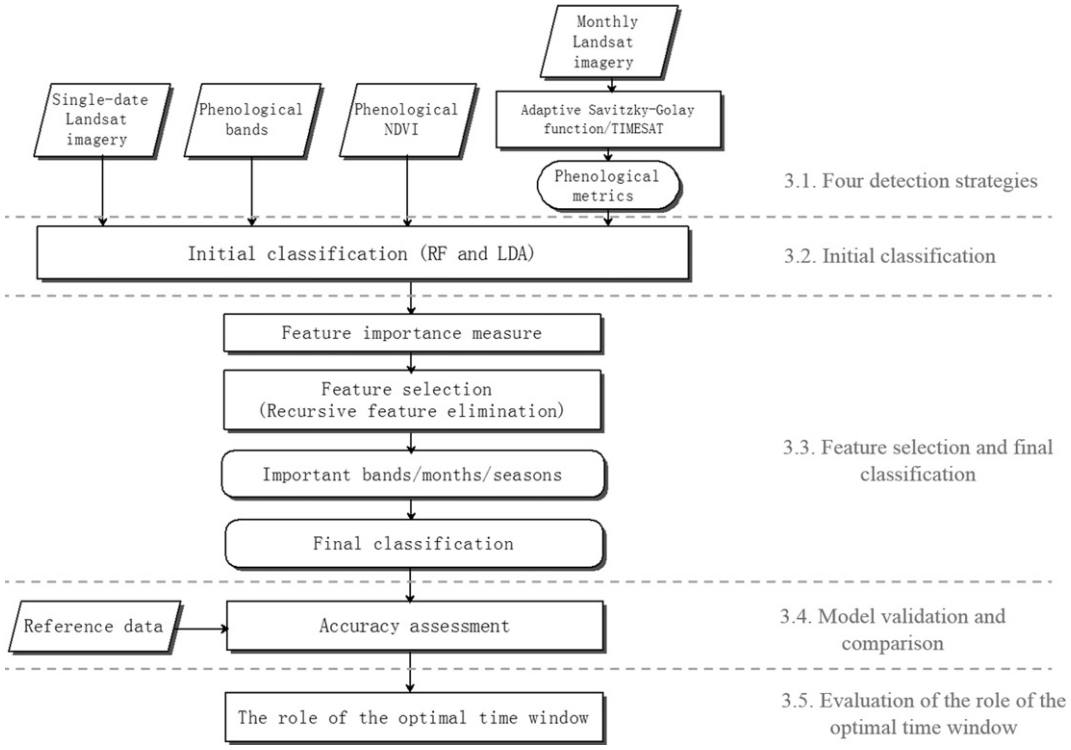

Fig. 3. Flowchart of the methodology to investigate the role of plant phenological trajectory traced by monthly Landsat time series in saltcedar mapping.

brown-down and senescence. The seasonal integrated NDVI is a widely used proxy for net primary production (Ruimy, Saugier, & Dedieu, 1994). The large seasonal integral is the cumulative NDVI in vegetation growth and indicates the vegetation production during the length of the growing season. The small seasonal integral, on the other hand, indicates seasonally active vegetation growth or productivity over the growing season. These phenological features constituted the phenological metrics that were used in the subsequent classification.

3.2. Initial classification

Initial classification of the four detection strategies was conducted using all candidate features (e.g., 72 features for the strategy of phenological bands). Two classification algorithms (random forest and linear discriminant analysis) were employed. As a non-parametric classification algorithm, random forest (RF) does not make assumptions about the underlying distributions of the data. It is an ensemble of a large number of decision trees. The construction of each decision tree is based on randomly selected features of a bootstrapped sample of training data (Breiman, 2001). For each individual tree, RF only searches across a random subset of input features to determine a split at each node, and the criterion for best splitting is frequently based on the Gini index to maximize the dissimilarity between classes (Breiman,

Table 2
Four detection strategies developed in this study.

Strategy	Description
Single-date Landsat imagery (baseline for comparison)	A single Landsat image (6 bands) was acquired on December 26, 2005, within the optimal time window to spectrally detect saltcedar.
Phenological bands	One Landsat image was acquired or interpolated in each month of the year 2005 (see Fig. 2 for details). Each Landsat image has 6 bands. The strategy contains 72 features (6 bands times 12 months).
Phenological NDVI	One Landsat image was acquired or interpolated in each month of the year 2005 (see Fig. 2 for details). The NDVI value was calculated for each Landsat image. The strategy contains 12 features (1 NDVI times 12 months).
Phenological metrics	Phenological metrics were extracted from the smoothed time series of monthly Landsat NDVI. The phenological metrics are composed of 11 representative phenological features, namely beginning of the growing season, end of the growing season, length of the growing season, base NDVI value, time of the peak growing season, peak NDVI value, amplitude, left derivative, right derivative, large seasonal integral, and small seasonal integral.

Table 3
Definition of phenological metrics.

Phenological metrics	Definition
Beginning of the growing season	The time for which the left edge has increased to 20% of the difference between the left minimum NDVI and the maximum NDVI.
End of the growing season	The time for which the right edge has decreased to 20% of the difference between the right minimum NDVI and the maximum NDVI.
Length of the growing season	The time window from the beginning to the end of the growing season.
Base NDVI value	The average of the left and right minimum value.
Time of the peak growing season	The mean value of the date for which the left edge has increased to 80% level and the right edge has decreased to 80% level.
Peak NDVI value	The largest NDVI value of the fitted function over the growing season.
Amplitude	The difference between the peak NDVI value and the base NDVI value.
Left derivative	The ratio of the difference between the left 20% and 80% levels to the corresponding time difference.
Right derivative	The ratio of the difference between the right 20% and 80% levels to the corresponding time difference.
Large seasonal integral	The area of the region between the fitted function and the zero level during the growing season.
Small seasonal integral	The area of the region between the fitted function and the base level during the growing season.

2001; Breiman, Friedman, Stone, & Olshen, 1984). The complement (out-of-bag) of the bootstrapped sample is used for evaluating the performance of RF. The class label of each unassigned pixel is determined by the majority voting of all the decision trees.

RF offers several advantages over traditional classification methods. The special characteristics of RF (i.e., random features and random samples) largely reduce the correlation between individual trees, increase the learnt pattern diversity, and enhance the capability of ensemble generalization (Pal, 2005). Owing to the strong law of large number, the generalization error always converges as the number of trees increases (Breiman, 1996). RF can thus effectively eliminate the potential model overfitting problem. Moreover, RF does not require dimensional reduction of input feature space. It can handle thousands of features without feature deletion, and measure the importance for each candidate feature. As an ensemble method, RF is robust to slight variation in input data, and not sensitive to noise. RF has been demonstrated to yield improved accuracy in comparison to other supervised classification methods (Chan & Paelinckx, 2008; Gislason, Benediktsson, & Sveinsson, 2006).

The RF algorithm was implemented with the randomForest package in R statistical software (Liaw & Wiener, 2002). Two parameters need to be defined in RF: the number of trees, and the number of random variables to split each node of the individual tree. It is desirable to use a large number of trees and a relatively small number of split variables (Breiman, 2001). In this study the number of trees was set to 1000, a number large enough to obtain an unbiased estimate of generalization errors. Once the error converges, the number of random split variables defined only affects the model accuracy slightly. A relatively small number of random variables can reduce the correlation between trees and enhance the generalization capability. The ensemble learning strategy can compensate for the decreased strength of the individual trees trained by limited random variables (Breiman, 2001). In this study, the number of random split variables was set to the square root of the total number of features, which is the standard setting of the randomForest package. The final class label assigned to each unknown pixel was the most frequent class of the total 1000 decision trees trained.

For comparison purposes, linear discriminant analysis (LDA) was also employed to classify the same dataset. LDA is a well-known, widely used supervised classifier that searches for linear combinations of input variables to best separate classes (Fisher, 1936). It seeks to find the optimal linear transformation by maximizing the ratio of the between-class variance to the within-class variance in the discriminant space (Venables & Ripley, 2013). As a parametric classifier, LDA assumes that classes follow multivariate normal distributions and have identical covariance matrices (i.e., homoscedasticity). LDA was implemented with the MASS package in R statistical software (Venables & Ripley, 2013).

3.3. Feature selection and final classification

With the initial classification result, the importance of candidate features could be measured. In RF, the feature importance was estimated in terms of the degradation of model prediction (i.e., mean decrease in accuracy), caused by the random permutation (Breiman, 2001). The values of a feature in the out-of-bag (OOB) samples were permuted randomly while other features were held constant. The modified OOB samples were passed down the decision tree to obtain new predictions. The prediction accuracy of the modified OOB samples was compared to that of the original OOB data, and the difference was averaged over all the trees grown in the forest. This mean decrease in prediction accuracy was then used to determine the importance of the feature in the classification process. As for LDA, the explanatory power of the feature can be estimated by the mean discriminant function coefficients. The standardized coefficient associated with the feature indicates the relative contribution of the feature to the discriminant function. For each feature, the weighted average of the standardized coefficients over all discriminant functions can be used to measure its overall contribution towards the discrimination between classes (Immitzer, Atzberger, & Koukal, 2012).

The recursive feature elimination algorithm was utilized in both classifiers to select important features (or months) in saltcedar mapping (Guyon, Weston, Barnhill, & Vapnik, 2002). The algorithm starts with all candidate features (e.g., 72 features for the strategy of phenological bands) in the model, and progressively eliminates one insignificant feature until the predefined size of feature subsets (i.e., one feature in this study) is achieved. In each iteration, it removes the least promising feature based on the feature importance measure (e.g., degradation of model prediction in RF), rebuilds the model with the features retained, recalculates the model accuracy (e.g., Kappa statistic), and remeasures the feature importance (but not for RF, see Svetnik, Liaw, Tong, & Wang, 2004). The algorithm is formulated to develop a parsimonious classification model that identifies the optimal subset of discriminatory features, while attaining the highest classification accuracy (Guyon et al., 2002). It helps in ascertaining which features (i.e., months and seasons) are desirable in modeling the differences between classes. The recursive feature elimination algorithm was implemented with the caret package in R statistical software, and the bootstrapping resampling method was incorporated in the algorithm to secure better estimates of the model performance during the selection process (Kuhn, 2008).

Final classification of the four proposed detection strategies was then conducted using the selected features. Compared to the initial classification with all candidate features, final classification could effectively improve the detection accuracy through using only the optimal subset of discriminatory features.

3.4. Model validation and comparison

The confusion matrix was constructed for each classification strategy with the testing samples to evaluate the model performance. Several measures were calculated from the confusion matrix: the overall accuracy, the Kappa statistic, the producer's and user's accuracies for each class (Congalton & Green, 2008). Furthermore, the McNemar's test was employed to compare the overall classification accuracies of different strategies in a statistically rigorous manner (Foody, 2004). It is a non-parametric test for evaluating the statistical significance of the difference between two classification results based on the same testing samples. For example, it can be used to test whether the classification result using the single-date image acquired within the optimal time window is significantly different from that using the phenological bands. The McNemar's test is based on the chi-square test statistic (Eq. (1)).

$$\chi^2 = \frac{(f_{12} - f_{21})^2}{f_{12} + f_{21}} \quad (1)$$

Here f_{12} denotes the number of testing samples correctly classified by the first classifier, but incorrectly classified by the second classifier. Similarly, f_{21} denotes the number of testing samples correctly classified by the second classifier, but incorrectly classified by the first classifier. The null hypothesis of the McNemar's test states that the two classifiers have the same error rate (i.e., $f_{12} = f_{21}$). The McNemar's test result follows the chi-square distribution with one degree of freedom.

3.5. Evaluation of the role of the optimal time window

As the optimal time window, December has been prioritized in monitoring the distribution of exotic saltcedar in the study area. Yet the quality of the image acquired during this period is not always assured. The few candidate images, limited by the 16-day revisit cycle of Landsat, may severely suffer from cloud contamination or atmospheric noise. To investigate the role of the optimal time window in saltcedar mapping,

the classification performance using the monthly Landsat imagery (i.e., phenological bands) was compared to that of 11 months' Landsat imagery (i.e., 11 months' bands). 11 months' Landsat imagery denote the same images as the ones of the monthly Landsat imagery, except the image acquired during the optimal time window (i.e., December). The importance of months and seasons in the 11 months' Landsat imagery was also evaluated using the recursive feature elimination algorithm. The performance of 11 months' Landsat time series can illustrate how important the image acquired in the optimal time window is in discriminating saltcedar from native species. It can also indicate how robust (or sensitive) the intra-annual time series analysis is to the lack of a single image.

4. Results

4.1. Classification accuracies of four detection strategies

As the baseline for benchmarking the Landsat-based time series analysis, the single-date Landsat image acquired within the optimal time window, with the RF classification algorithm, yielded the overall classification accuracy of 83.35% and the Kappa statistic of 0.71 (Table 4). The corresponding producer's and user's accuracies of the saltcedar class were 87.04% and 81.59%, respectively. Three competing temporal mapping strategies were explored in this study to capture the phenological dynamics of plants. Compared to the single-date Landsat image, the phenological bands, with the RF classifier, achieved a considerably improved classification accuracy. The overall classification accuracy increased from 83.35% to 88.54%, and the Kappa statistic rose from 0.71 to 0.80. The McNemar's chi-square test rejected the null hypothesis that the error rates for these two strategies were the same ($p < 0.001$), and indicated that the strategy of phenological bands did yield a more accurate classification. However, as for the phenological NDVI (or phenological metrics), the model performance was not significantly improved. As a widely recognized vegetation index, NDVI is primarily developed to measure the photosynthetic activities and greenness of plants, and is calculated based on the red band (band 3) and the near-infrared band (band 4) of Landsat imagery. Compared to the phenological bands, the decreased performance using phenological NDVI (or derived phenological metrics) may be caused by the reduced amount of critical land cover information obtained in each month. The classification results from the LDA algorithm exhibited similar patterns among the four detection strategies.

There were three classes (i.e., saltcedar, native species, and other) considered in this study. By scrutinizing the commission and omission errors of each class, we found that the strategy of phenological bands performed better than that of the single-date imagery for all the classes (Fig. 4). Compared to the accuracies of the singe-date imagery, the user's accuracy of the saltcedar class increased by about 6–9% and the producer's accuracy of native species increased by >10% through using the phenological bands. The improved accuracy could also be reflected in the confusion matrices constructed for these two classification strategies (Tables S2 and S3). The comparisons revealed that the areas saltcedar occupied were overestimated with the traditional single-image-based detection strategy, mainly due to the spectral confusion between saltcedar and native species. Concurrently, the areas inhabited by native species were underestimated notably. The intra-annual phenological information incorporated by the phenological bands was beneficial to correct these confusion errors.

The classification results indicated that the RF classifier consistently performed better than the LDA classifier in terms of the overall accuracy and McNemar's chi-square test statistic in all classification strategies (Table 4). As for each individual class, the RF classifier yielded higher classification accuracy than LDA with respect to the producer's and user's accuracies in almost every scenario (Fig. 4). LDA is a parametric classifier and need test the assumptions of the data. In our study the classes were mostly normally distributed and had similar covariance matrices according to the Box's M test, which led to similar patterns of detection results between RF and LDA. Yet for the detection strategy of phenological metrics, transformation (e.g., logarithm) of features was needed to meet the assumptions of LDA. In contrast, RF is a non-parametric classifier and does not assume the normal distribution of the data. It is robust to the influence of the noise and outliers in the data, and does not suffer from overfitting as other multivariate approaches (e.g., LDA) do. Unlike the traditional classification scheme, the ensemble learning strategy of RF, with the majority voting decision rule, effectively increases the learnt pattern diversity and reduces the generalization error. Compared to LDA, RF is more capable of handling high dimensional feature spaces. Given the advantages and improved accuracy achieved, RF was mainly scrutinized for subsequently identifying the important months in remotely detecting saltcedar (Section 4.2) and evaluating the role of the optimal time window in the Landsat time series (Section 4.3).

4.2. Important months and seasons in saltcedar detection

With the most powerful detection strategy (i.e., phenological bands), the recursive feature elimination algorithm was employed in RF to investigate influential months and seasons in characterizing and mapping the saltcedar. The algorithm started with all 72 bands (6 bands per month) in the model. It eliminated the least promising band in each iteration based on the feature importance measure (i.e., mean decrease in accuracy), until only one band remained in the model. The overall accuracy of the model varied from 66.42% to 88.54%, depending on the number of bands used. The highest accuracy (i.e., the overall accuracy of 88.54% and the Kappa statistic of 0.80) was achieved when there were 68 bands constructing the RF. Among these selected bands, the top crucial bands were colored in dark red, while the least decisive bands were shown in dark blue (Fig. 5). The essential bands, indicated by the red and orange color, were mostly distributed in October, November, and December.

In the feature elimination process, the feature importance scores of these selected bands were calculated based on the mean decrease in the OOB accuracy, caused by the feature permutation. The higher score indicated that the corresponding band (or feature) contributed more to the RF classification model. For each month, the average score of the bands was calculated to gauge the contribution of the month to the class separability and classification success (Fig. 6). The importance of the month denoted by the average score in Fig. 6 was consistent with

Table 4
Classification accuracies of the four proposed detection strategies.

Strategy	RF				LDA				McNemar's test to compare RF and LDA (p-value)
	Overall accuracy (%)	Kappa statistic	Saltcedar		Overall accuracy (%)	Kappa statistic	Saltcedar		
			Producer's accuracy (%)	User's accuracy (%)			Producer's accuracy (%)	User's accuracy (%)	
Single-date Landsat imagery	83.35	0.71	87.04	81.59	80.20	0.67	89.73	71.74	51.77 ($p < 0.001$)
Phenological bands	88.54	0.80	91.22	87.51	84.91	0.74	90.99	82.65	85.50 ($p < 0.001$)
Phenological NDVI	83.39	0.71	90.09	81.48	79.33	0.64	88.42	73.79	95.73 ($p < 0.001$)
Phenological metrics	79.15	0.64	87.64	74.18	75.73	0.58	86.69	69.94	65.96 ($p < 0.001$)

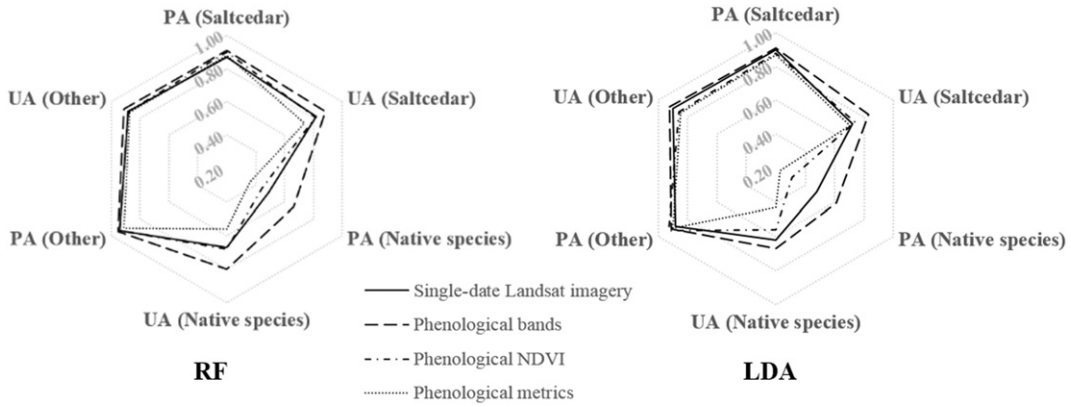

Fig. 4. The producer's accuracy (PA) and user's accuracy (UA) of three classes using RF (left) and LDA (right).

the distribution of the band importance in Fig. 5. The most influential month was December, with an average score of 14.07. Almost all the bands contained the valuable information in discriminating the classes. This explained why December was deemed as the optimal time window in the study area. However, October and November also were perceived as important, with average scores of 12.15 and 11.37, respectively. In late October, saltcedar leaves enter the senescence stage and start to change colors. These top three months are all closely related to the leaf coloration and senescence process of saltcedar. The Landsat time series is beneficial to capture the gradual change of leaf color during the senescence stage and utilize this phenological information to discriminate saltcedar from native species. Besides the important months mentioned above, the feature importance measure also indicated that the rest of months, such as August and June, can help in detecting saltcedar.

4.3. The role of the optimal time window in saltcedar detection

To investigate the role of the optimal time window in saltcedar mapping, 11 months' (except December) Landsat bands were classified with the RF classification algorithm. Compared to the phenological bands (i.e., 12 months' bands), the overall classification accuracy of 11 months' bands decreased by 0.65% (from 88.54% to 87.89%), and the Kappa statistic decreased by 0.01 (from 0.80 to 0.79) (Table 5). The McNemar's test result indicated that the difference between these two classification accuracies was statistically significant ($p < 0.05$), given the large sample size of the testing data. Despite the statistically significant difference, the model performance of the 11 months' bands did not deteriorate much. It still significantly improved the model accuracy compared to that of the single-date image strategy, by increasing the overall accuracy from 83.35% to 87.89%, and the Kappa statistic from 0.71 to 0.79. This notable increase in the model accuracy indicated that the Landsat time series analysis is relatively robust and insensitive to the lack of the image acquired within the optimal time window. The temporal phenological information possessed by the Landsat time series can be used to compensate for the lack of distinct features offered by a single-date image, and mitigate the influence of the image unavailability during this period.

By comparing the confusion matrices constructed for the phenological bands and 11 months' bands, we found that incorporation of the bands acquired in December into the Landsat time series mainly increased the producer's accuracy of native species (Table 6). Out of 1367 reference pixels of native species, 842 were correctly classified with 11 months' bands. This number increased to 900 when the bands in December were taken into account. In other words, despite the relatively high accuracy achieved with 11 months' bands, the areas inhabited by native species were underestimated. The image acquired within the optimal time window was beneficial to correct this omission error. The incorporation of the distinct features during this period

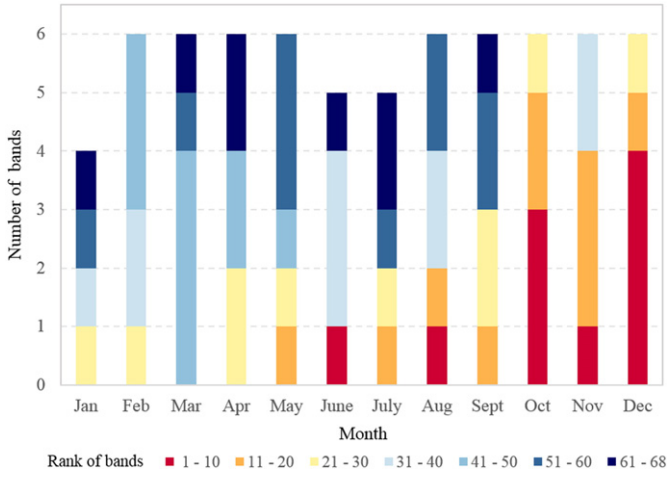

Fig. 5. Contribution of the bands in each month to the classification with the strategy of phenological bands. The top 10 important bands selected by the recursive feature elimination algorithm were colored in dark red, while the least decisive bands were colored in dark blue.

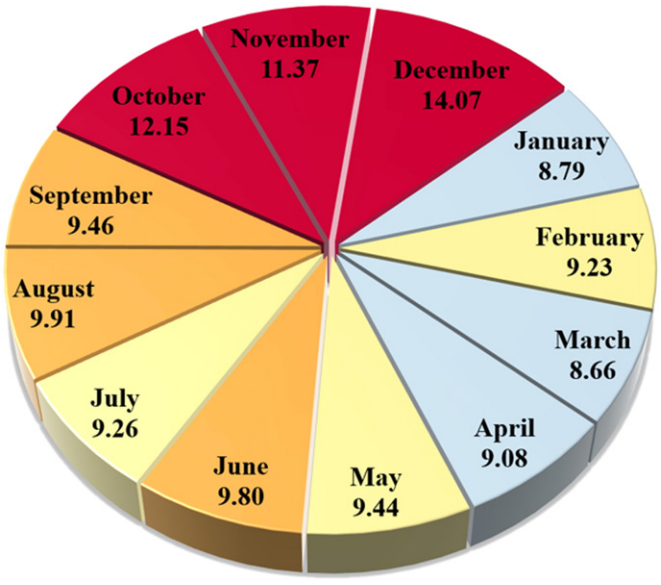

Fig. 6. Contribution of each month to the classification with the strategy of phenological bands through calculating the average score of the feature importance.

Table 5
Classification accuracies of the Landsat time series with or without the image acquired in December.

Scenario	Overall accuracy (%)	Kappa statistic	Saltcedar	
			Producer's accuracy (%)	User's accuracy (%)
Single-date Landsat imagery	83.35	0.71	87.04	81.59
Phenological bands	88.54	0.80	91.22	87.51
11 months' bands	87.89	0.79	91.28	86.43

helped further distinguish saltcedar from native species, owing to their leaf color differences.

With the recursive feature elimination algorithm, the feature importance in the RF classification using only 11 months' bands was explored. Out of 66 bands (i.e., 11 months with 6 bands per month), 53 bands were selected with the algorithm to achieve the highest classification accuracy (Fig. 7). Almost all the months over the growing season carried valuable information in discriminating the plants in the study area. The average score of the feature importance was calculated for each month (Fig. 8). The results indicated that, without the month of December, November contributed the most to the prediction accuracy of the RF classifier, followed by October (Fig. 7 and Fig. 8). The rest of the months, such as August, September, July, June, and May, also encompassed discriminant phenological information (e.g., flowering and seed production) that is useful to characterize the plants.

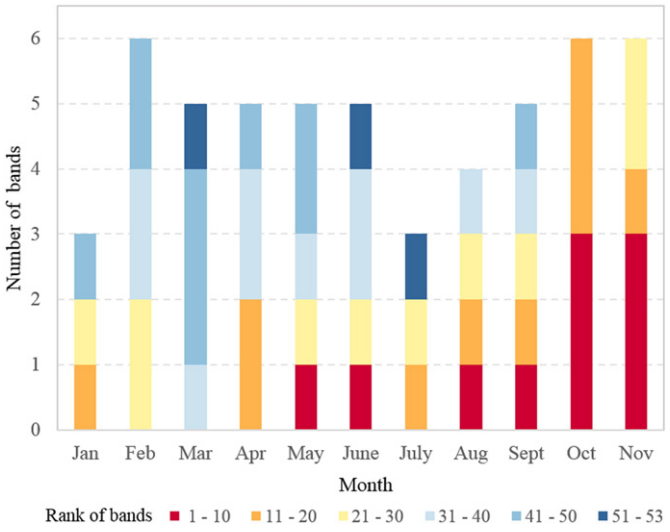

Fig. 7. Contribution of the bands in each month (except December) to the classification with 11 months' bands. The top 10 important bands selected by the recursive feature elimination algorithm were colored in dark red, while the least decisive bands were colored in dark blue.

5. Discussion

A continuing challenge in conducting saltcedar mapping in the study area is the spectral confusion between saltcedar and native shrubs. The single-date-based detection strategy, with the image acquired during the saltcedar leaf senescence stage, has been prioritized in previous studies to capture the leaf color difference of these shrub plants. At the Landsat scale, this operational strategy is relatively straightforward to implement, but it fails to accommodate the phenological variation within class. For example, saltcedar in various phenological stages (e.g., leaf on, leaf senescence, and leaf off) may exist in an image. Yet the single-date Landsat imagery acquired in this study is only effective in detecting the senescent saltcedar. Though there was a lack of studies assessing the influence of within-class phenological variation on the mapping success, this variation did notably affect the detection accuracy of saltcedar (see Section 4.1). Additionally, the timing of phenological events (e.g., leaf senescence) is affected by a combination of biotic and abiotic factors, such as regional climate, topography, latitudinal gradients, and species interactions in ecological systems (Richardson et al., 2013). As a result, the timing of leaf senescence varies over space and time (Friedman, Roelle, & Cade, 2011). It is difficult to repeatedly determine the optimal time window for detecting saltcedar across years and locations without the expert knowledge. This single-date-based detection strategy thus lacks the generalization capability to conduct the long-term, regional-scale monitoring of saltcedar.

The role of the Landsat time series was evaluated from three aspects: phenological bands, phenological NDVI, and phenological metrics. The detection strategy that remarkably improved the mapping accuracy was through the utilization of the phenological bands. This phenology-based detection strategy, compared to the commonly used single-date-detection strategy, presented several advantages. First, the phenological bands could better characterize the leaf senescence process of saltcedar. Plant phenology is affected by various abiotic and biotic factors. These factors, as a consequence, make it challenging to pinpoint the exact week (or month) for observing the saltcedar leaf senescence, especially in spatially heterogeneous landscapes. In this study, October, November, and December were selected as the most crucial in distinguishing saltcedar from native species. These selected months are all closely related to the growth cessation and leaf senescence stage of saltcedar (Everitt & Deloach, 1990; Yang et al., 2013; Diao & Wang 2016). Compared to a single-date image, the Landsat time series is more capable of accommodating the phenological variation within class. Hence this proposed detection strategy increased the user's accuracy of saltcedar and the producer's accuracy of native species.

Another advantage of this proposed strategy is that the phenological bands carry rich information about the intra-annual phenological trajectory of plant development. This phenology-based detection strategy could trace the temporal variation in spectral reflectance of plants over the course of the growing season. It takes into account various phenological stages and biological events, rather than only the time window of leaf senescence. In this study, besides the late fall and early winter period (i.e., October, November, and December), the rest of the months also contributed discriminatory power between mapped classes. Several bands in May, June, August, and September were selected as important features in saltcedar mapping, owing to the ability to capture phenological differences in vegetation. In the mapping year, saltcedar begins blooming in late May and achieves the peak of flowering in June. The flowers produced by saltcedar are typically

Table 6
Confusion matrices constructed for the monthly Landsat bands and 11 months' bands with the RF classifier.

		Phenological bands						11 months' bands			
		Reference data						Reference data			
		Saltcedar	Native	Other	Total			Saltcedar	Native	Other	Total
Classified data	Saltcedar	1528	180	38	1746	Classified data	Saltcedar	1529	201	39	1769
	Native	86	900	141	1127		Native	81	842	128	1051
	Other	61	287	3697	4045		Other	65	324	3709	4098
	Total	1675	1367	3876	6918		Total	1675	1367	3876	6918

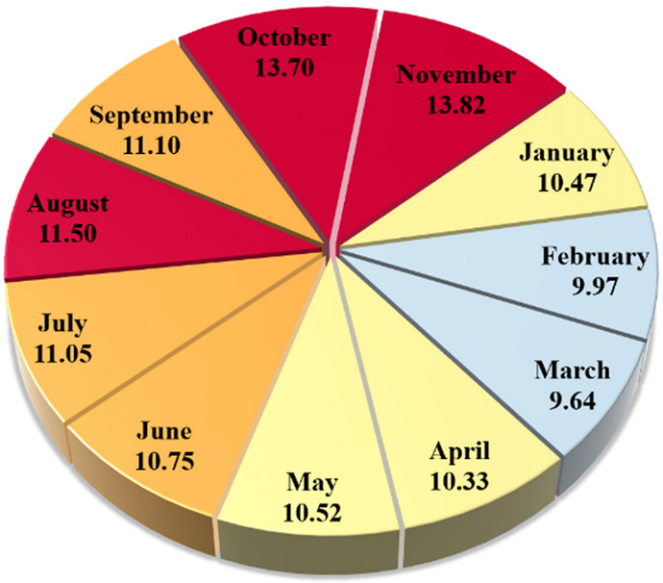

Fig. 8. Contribution of each month to the classification with 11 months' bands through calculating the average score of the feature importance.

pinkish-white, and can be well distinguished from the yellowish-green flowers of mesquite. In September, the light green foliage of saltcedar has been found to be different from the darker green foliage of mesquite, and the light-brown color of flowering willow (Everitt & Deloach, 1990). Therefore, this strategy can enhance the discrimination between plants that exhibit distinct phenological patterns, though the plants may share similar spectral characteristics at a single time point.

The strategy of phenological bands is also relatively robust to the lack of a single Landsat image. The study demonstrated that the mapping accuracy did not deteriorate much without the image acquired in December. This detection strategy, therefore, can help overcome the limits caused by a single image during certain time periods and add credibility to the repetitive mapping of saltcedar distribution over time. However, to extend the strategy to other targeted years, the inter-annual phenological variation of plants need to be taken into account. Inter-annual climate variability and fluctuations may alter the timing of phenological events. For example, warm springtime temperatures can yield early bud-break and leaf flushing. To formulate a more generalized and stable multi-year detection model, the time lag, due to the shift of phenological timing, need to be incorporated in future research (Fisher, Mustard, & Vadeboncoeur, 2006). The MODIS vegetation phenology products from the US Geological Survey, along with key phenological stages discovered by this study, can help determine the time lag and guide the selection of relevant images. In this study, the geographical area for developing the phenology-based detection strategy is limited to the extent of the AISA image to secure high-quality training and testing data. Despite the relatively restricted geographical area, the proposed strategy takes into account the phenological variation of plants caused by environmental differences (e.g., topography) (Table 1). It is expected that the proposed strategy can be extended to geographical areas that share similar species composition, though the time lag caused by the latitudinal difference may also need to be incorporated. In future studies, it is desired to refine the proposed strategy by collecting high quality reference data (e.g., field data designed at the Landsat scale) spanning diverse geographical regions to formulate a more robust spatially generalized detection model. We admitted that sometimes it is difficult to acquire sufficient cloud-free Landsat images to formulate this phenology-based detection strategy. Under these circumstances, pinpointing several months that can capture the key phenological differences between plants may also help in improving the classification performance.

The other two developed strategies (i.e., phenological NDVI and phenological metrics) did not improve the mapping accuracy of saltcedar in this study. Compared to the phenological bands, the phenological NDVI carries less information of land cover types in each month. Yet in this study, almost all the bands from October to December play a role in discriminating saltcedar from native shrubs (Fig. 5 and Fig. 7). Though NDVI has been demonstrated to be an effective measure to separate vegetated areas from non-vegetated regions, its power to distinguish various shrub plants still needs to be examined. Compared to the traditional time series studies using satellites of high temporal resolution (e.g., MODIS), the finer spatial resolution of Landsat in this study presents unique opportunities to distinguish the shrub plants along spatially heterogeneous riparian corridors. However, the relatively coarse temporal resolution of Landsat may not achieve the full potential of NDVI time series in depicting the plant phenology. To better evaluate the role of these two strategies, in future studies, it will be beneficial to fuse the satellite imagery of high temporal resolution (e.g. MODIS) with Landsat imagery to construct dense time series of synthetic Landsat data. Several data fusion algorithms, such as the Spatial and Temporal Adaptive Reflectance Fusion Model (STARFM), and the Spatial and Temporal Data Fusion Approach (STDFA), have been developed for this purpose (Gao, Masek, Schwaller, & Hall, 2006; Wu, Niu, Wang, Wu, & Wang, 2012). It will also be beneficial to build the NDVI time series through combining the Landsat imagery with the upcoming ESA's Sentinel-2 data.

As the third most frequently occurring woody riparian plant, saltcedar has expanded its distribution in western riparian zones considerably over the past century. The landscapes along the riparian corridors, as a consequence, have been transformed enormously. The rapid colonization of saltcedar has been indicted for the depletion of river flows, the reduction of ecosystem diversity, etc. This negative perception of saltcedar in the riparian ecosystems has recently been challenged by new research findings and called for reevaluation (see Stromberg et al., 2009). The reevaluation, however, suffers from the lack of distributional maps and dynamic changes of saltcedar over time. Accurate mapping of saltcedar in western riparian zones is thus urgently important to provide a thorough understanding of the cause of vegetation change, and ecological effects of non-native species. In recent years, the advancement of satellite technologies (i.e., airborne hyperspectral sensors) and classification algorithms has facilitated the detection of saltcedar at local scales. Yet the remotely-sensed, regional-scale mapping of this exotic plant populating diverse riparian corridors still presents many challenges and limitations. To alleviate the limitations, in this study, several intra-annual phenology-based detection strategies were developed using the Landsat time series. With the freely available historical archives and continuing acquisitions of Landsat imagery, these strategies exhibit great potential in monitoring the spatial and temporal dynamics of saltcedar, and guiding the systemic restoration of the riparian ecosystems.

6. Conclusions

The riparian zones in southwestern US have undergone significant changes over the last century, due to the rapid expansion and colonization of saltcedar. Mapping the geographic distribution of saltcedar at the regional scale is urgently needed to evaluate its role and ecological effects in spatially diverse riparian ecosystems. In this study, several phenology-based detection strategies (i.e., phenological bands, phenological NDVI, and phenological metrics) that could track the intra-annual plant phenological trajectory were developed with monthly time series of Landsat imagery. The recursive feature elimination algorithm was implemented in this process to identify crucial months and seasons in distinguishing saltcedar from other riparian vegetation. The importance of the optimal time window in the Landsat time series was also explored. Compared to the commonly used single-date-based detection strategy, the strategy of phenological bands largely increased

the detection accuracy, especially the user's accuracy of saltcedar and the producer's accuracy of native species. The drastic improvement in plant discrimination can be attributed to its capability of carrying rich phenological and spectral information of plants over the entire growing season. The late fall and early winter period (i.e., October, November, and December) was found to be the most crucial stage in differentiating riparian vegetation in the study area. Yet several other months (e.g., August, September, May, and June) also contributed discriminatory power between mapped classes. Despite the important role of the optimal time window, the strategy of phenological bands was found to be relatively robust to the lack of a single Landsat image. With the unprecedented opportunities provided by Landsat imagery, it is believed that this proposed temporal phenology-based detection strategy is promising to facilitate the long-term, region-wide monitoring of saltcedar.

Appendix A. Supplementary data

Supplementary data associated with this article can be found in the online version. These data include three tables that present the confusion matrices for evaluating the classification performance.

References

Beck, P. S., Atzberger, C., Høgda, K. A., Johansen, B., & Skidmore, A. K. (2006). Improved monitoring of vegetation dynamics at very high latitudes: A new method using MODIS NDVI. *Remote Sensing of Environment*, *100*, 321–334.

Bradley, B. A. (2014). Remote detection of invasive plants: A review of spectral, textural and phenological approaches. *Biological Invasions*, *16*, 1411–1425.

Breiman, L. (1996). Bagging predictors. *Machine Learning*, *24*, 123–140.

Breiman, L. (2001). Random forests. *Machine Learning*, *45*, 5–32.

Breiman, L., Friedman, J., Stone, C. J., & Olshen, R. A. (1984). *Classification and regression trees*. CRC Press.

Chan, J. C. -W., & Paelinckx, D. (2008). Evaluation of Random Forest and Adaboost tree-based ensemble classification and spectral band selection for ecotope mapping using airborne hyperspectral imagery. *Remote Sensing of Environment*, *112*, 2999–3011.

Congalton, R. G., & Green, K. (2008). *Assessing the accuracy of remotely sensed data: principles and practices*. CRC Press.

Di Tomaso, J. M. (1998). Impact, biology, and ecology of saltcedar (*Tamarix* spp.) in the southwestern United States. *Weed Technology*, 326–336.

Diao, C., & Wang, L. (2014). Development of an invasive species distribution model with fine-resolution remote sensing. *International Journal of Applied Earth Observation and Geoinformation*, *30*, 65–75.

Diao, C., & Wang, L. (2016). Temporal partial unmixing of exotic salt cedar using Landsat time series. *Remote Sensing Letters*, *7*, 466–475.

Engel-Wilson, R. W., & Ohmart, R. D. (1978). Floral and attendant faunal changes on the lower Rio Grande between Fort Quitman and Presidio, Texas. *Proceedings of the National Symposium for Protection and Management of Floodplain Wetlands* (pp. 139–147).

Evangelista, P. H., Stohlgren, T. J., Morisette, J. T., & Kumar, S. (2009). Mapping invasive tamarisk (*Tamarix*): A comparison of single-scene and time-series analyses of remotely sensed data. *Remote Sensing*, *1*, 519–533.

Everitt, J., & Deloach, C. (1990). Remote sensing of Chinese tamarisk (*Tamarix chinensis*) and associated vegetation. *Weed Science*, 273–278.

Fisher, R. A. (1936). The use of multiple measurements in taxonomic problems. *Annals of Eugenics*, *7*, 179–188.

Fisher, J. I., Mustard, J. F., & Vadeboncoeur, M. A. (2006). Green leaf phenology at Landsat resolution: Scaling from the field to the satellite. *Remote Sensing of Environment*, *100*, 265–279.

Follstad Shah, J. J., Dahm, C. N., Gloss, S. P., & Bernhardt, E. S. (2007). River and riparian restoration in the Southwest: Results of the National River Restoration Science Synthesis Project. *Restoration Ecology*, *15*, 550–562.

Foody, G. M. (2004). Thematic map comparison. *Photogrammetric Engineering & Remote Sensing*, *70*, 627–633.

Friedman, J. M., Auble, G. T., Shafroth, P. B., Scott, M. L., Merigliano, M. F., Freehling, M. D., & Griffin, E. R. (2005). Dominance of non-native riparian trees in western USA. *Biological Invasions*, *7*, 747–751.

Friedman, J. M., Roelle, J. E., & Cade, B. S. (2011). Genetic and environmental influences on leaf phenology and cold hardiness of native and introduced riparian trees. *International Journal of Biometeorology*, *55*, 775–787.

Gao, F., Masek, J., Schwaller, M., & Hall, F. (2006). On the blending of the Landsat and MODIS surface reflectance: Predicting daily Landsat surface reflectance. *Geoscience and Remote Sensing, IEEE Transactions on*, *44*, 2207–2218.

Gislason, P. O., Benediktsson, J. A., & Sveinsson, J. R. (2006). Random forests for land cover classification. *Pattern Recognition Letters*, *27*, 294–300.

Glenn, E. P., & Nagler, P. L. (2005). Comparative ecophysiology of *Tamarix ramosissima* and native trees in western US riparian zones. *Journal of Arid Environments*, *61*, 419–446.

Guyon, I., Weston, J., Barnhill, S., & Vapnik, V. (2002). Gene selection for cancer classification using support vector machines. *Machine Learning*, *46*, 389–422.

Hamada, Y., Stow, D. A., Coulter, L. L., Jafolla, J. C., & Hendricks, L. W. (2007). Detecting Tamarisk species (*Tamarix* spp.) in riparian habitats of Southern California using high spatial resolution hyperspectral imagery. *Remote Sensing of Environment*, *109*, 237–248.

Hart, C. R., White, L. D., McDonald, A., & Sheng, Z. (2005). Saltcedar control and water salvage on the Pecos River, Texas, 1999–2003. *Journal of Environmental Management*, *75*, 399–409.

He, K. S., Rocchini, D., Neteler, M., & Nagendra, H. (2011). Benefits of hyperspectral remote sensing for tracking plant invasions. *Diversity and Distributions*, *17*, 381–392.

Hufkens, K., Friedl, M., Sonnentag, O., Braswell, B. H., Milliman, T., & Richardson, A. D. (2012). Linking near-surface and satellite remote sensing measurements of deciduous broadleaf forest phenology. *Remote Sensing of Environment*, *117*, 307–321.

Hultine, K. R., Belnap, J., Van Riper Iii, C., Ehleringer, J. R., Dennison, P. E., Lee, M. E., ... West, J. B. (2009). Tamarisk biocontrol in the western United States: Ecological and societal implications. *Frontiers in Ecology and the Environment*, *8*, 467–474.

Immitzer, M., Atzberger, C., & Koukal, T. (2012). Tree species classification with random forest using very high spatial resolution 8-band WorldView-2 satellite data. *Remote Sensing*, *4*, 2661–2693.

Ji, W., & Wang, L. (2016). Phenology-guided saltcedar (Tamarix spp.) mapping using Landsat TM images in western US. *Remote Sensing of Environment*, *173*, 29–38.

Jönsson, P., & Eklundh, L. (2002). Seasonality extraction by function fitting to time-series of satellite sensor data. *Geoscience and Remote Sensing, IEEE Transactions on*, *40*, 1824–1832.

Jönsson, P., & Eklundh, L. (2004). TIMESAT—A program for analyzing time-series of satellite sensor data. *Computers & Geosciences*, *30*, 833–845.

Kerr, J. T., & Ostrovsky, M. (2003). From space to species: Ecological applications for remote sensing. *Trends in Ecology & Evolution*, *18*, 299–305.

Kruse, F., Lefkoff, A., Boardman, J., Heidebrecht, K., Shapiro, A., Barloon, P., & Goetz, A. (1993). The spectral image processing system (SIPS)—Interactive visualization and analysis of imaging spectrometer data. *Remote Sensing of Environment*, *44*, 145–163.

Kuhn, M. (2008). Building predictive models in R using the caret package. *Journal of Statistical Software*, *28*, 1–26.

Lass, L. W., Prather, T. S., Glenn, N. F., Weber, K. T., Mundt, J. T., & Pettingill, J. (2009). *A review of remote sensing of invasive weeds and example of the early detection of spotted knapweed (Centaurea maculosa) and babysbreath (Gypsophila paniculata) with a hyperspectral sensor.*

Liaw, A., & Wiener, M. (2002). Classification and regression by randomForest. *R News*, *2*, 18–22.

Lieth, H. (1974). Purposes of a phenology book. *Phenology and seasonality modeling* (pp. 3–19). Springer.

Masek, J. G., Vermote, E. F., Saleous, N. E., Wolfe, R., Hall, F. G., Huemmrich, K. F., ... Lim, T. -K. (2006). A Landsat surface reflectance dataset for North America, 1990–2000. *Geoscience and Remote Sensing Letters, IEEE*, *3*, 68–72.

Morisette, J. T., Jarnevich, C. S., Ullah, A., Cai, W., Pedelty, J. A., Gentle, J. E., ... Schnase, J. L. (2006). A tamarisk habitat suitability map for the continental United States. *Frontiers in Ecology and the Environment*, *4*, 11–17.

Morisette, J. T., Richardson, A. D., Knapp, A. K., Fisher, J. I., Graham, E. A., Abatzoglou, J., ... Hanes, J. M. (2008). Tracking the rhythm of the seasons in the face of global change: Phenological research in the 21st century. *Frontiers in Ecology and the Environment*, *7*, 253–260.

Nagler, P. L., Glenn, E. P., Jarnevich, C. S., & Shafroth, P. B. (2011). Distribution and abundance of saltcedar and Russian olive in the western United States. *Critical Reviews in Plant Sciences*, *30*, 508–523.

Narumalani, S., Mishra, D. R., Burkholder, J., Merani, P. B., & Willson, G. (2006). A comparative evaluation of ISODATA and spectral angle mapping for the detection of saltcedar using airborne hyperspectral imagery. *Geocarto International*, *21*, 59–66.

Pal, M. (2005). Random forest classifier for remote sensing classification. *International Journal of Remote Sensing*, *26*, 217–222.

Peterson, E. (2005). Estimating cover of an invasive grass (Bromus Tectorum) using tobit regression and phenology derived from two dates of Landsat ETM+ data. *International Journal of Remote Sensing*, *26*, 2491–2507.

Rapinel, S., Bouzillé, J. -B., Oszwald, J., & Bonis, A. (2015). Use of bi-seasonal Landsat-8 imagery for mapping marshland plant community combinations at the regional scale. *Wetlands*, *35*, 1043–1054.

Richardson, A. D., Keenan, T. F., Migliavacca, M., Ryu, Y., Sonnentag, O., & Toomey, M. (2013). Climate change, phenology, and phenological control of vegetation feedbacks to the climate system. *Agricultural and Forest Meteorology*, *169*, 156–173.

Ruimy, A., Saugier, B., & Dedieu, G. (1994). Methodology for the estimation of terrestrial net primary production from remotely sensed data. *Journal of Geophysical Research-All Series*, *99*, 5263.

Rundquist, B., & Brookman, D. (2007). Spectral characterization of the invasive shrub saltcedar (*Tamarix* spp.) in North Dakota. *Geocarto International*, *22*, 63–72.

Shafroth, P. B., Cleverly, J. R., Dudley, T. L., Taylor, J. P., Riper, C. V., III, Weeks, E. P., & Stuart, J. N. (2005). Control of *Tamarix* in the western United States: Implications for water salvage, wildlife use, and riparian restoration. *Environmental Management*, *35*, 231–246.

Silván-Cárdenas, J., & Wang, L. (2010). Retrieval of subpixel *Tamarix* canopy cover from Landsat data along the Forgotten River using linear and nonlinear spectral mixture models. *Remote Sensing of Environment*, *114*, 1777–1790.

Singh, N., & Glenn, N. F. (2009). Multitemporal spectral analysis for cheatgrass (*Bromus tectorum*) classification. *International Journal of Remote Sensing*, *30*, 3441–3462.

Stromberg, J. C., Chew, M. K., Nagler, P. L., & Glenn, E. P. (2009). Changing perceptions of change: The role of scientists in Tamarix and river management. *Restoration Ecology*, *17*, 177–186.

Svetnik, V., Liaw, A., Tong, C., & Wang, T. (2004). Application of Breiman's random forest to modeling structure-activity relationships of pharmaceutical molecules. *Multiple Classifier Systems* (pp. 334–343). Springer.

Tan, B., Morisette, J. T., Wolfe, R. E., Gao, F., Ederer, G., Nightingale, J., & Pedelty, J. (2011). An enhanced TIMESAT algorithm for estimating vegetation phenology metrics from MODIS data. *Selected Topics in Applied Earth Observations and Remote Sensing, IEEE Journal of, 4*, 361–371.

Venables, W. N., & Ripley, B. D. (2013). *Modern applied statistics with S-PLUS*. Springer Science & Business Media.

Wang, L., Silván-Cárdenas, J. L., Yang, J., & Frazier, A. E. (2013). Invasive saltcedar (Tamarisk spp.) distribution mapping using multiresolution remote sensing imagery. *The Professional Geographer, 65*, 1–15.

Wang, L., & Zhang, S. (2014). Incorporation of texture information in a SVM method for classifying salt cedar in western China. *Remote Sensing Letters, 5*, 501–510.

Wu, M., Niu, Z., Wang, C., Wu, C., & Wang, L. (2012). Use of MODIS and Landsat time series data to generate high-resolution temporal synthetic Landsat data using a spatial and temporal reflectance fusion model. *Journal of Applied Remote Sensing, 6* (063507-063501-063507-063513).

Yang, C., Everitt, J. H., & Fletcher, R. S. (2013). Evaluating airborne hyperspectral imagery for mapping saltcedar infestations in west Texas. *Journal of Applied Remote Sensing, 7*, 073556.

Zavaleta, E. (2000). Valuing ecosystem services lost to *Tamarix* invasion in the United States. *Invasive species in a changing world* (pp. 261–300).

Zhang, X., Friedl, M. A., Schaaf, C. B., Strahler, A. H., Hodges, J. C., Gao, F., ... Huete, A. (2003). Monitoring vegetation phenology using MODIS. *Remote Sensing of Environment, 84*, 471–475.